Proceedings of the
46th IEEE Conference on Decision and Control
New Orleans, LA, USA, Dec. 12-14, 2007

Adaptive–Repetitive Control of a Hard Disk Drive

Néstor O. Pérez Arancibia, Chi-Ying Lin, Tsu-Chin Tsao and James S. Gibson

Abstract— **This paper presents a control scheme intended to target both the non–repeatable and repeatable runout disturbances affecting the dynamics of a *hard disk drive* (HDD). The design can be broken up into three stages. The first stage consists of a LTI feedback controller designed using classical techniques. The second stage consists of a RLS–based adaptively tuned controller. Finally, the last stage incorporates a new controller which integrates repetitive and adaptive elements. The repetitive part of this controller allows us to target specific periodic disturbances visible in the disturbance spectrum. The adaptive part is intended to cancel the inter–notch stochastic disturbances. The key element in this design is the formulation of an appropriate optimization problem, solvable recursively by the use of some of the available adaptive–filtering algorithms. Experimental results obtained from the implementation of this method in a commercial HDD demonstrates the effectiveness of this approach.**

I. Introduction

The control of *hard disk drives* (HDD) has attracted the attention of many researchers for many years. Typically, two kind of control problems have been defined: track–seeking and track–following. The former deals with the motion control of the head between tracks, the latter with maintaining the head on the center of the HDD track. In this paper we focus on track–following.

It has been reported that track–following can be thought of as an output disturbance rejection problem [1], [2], [3]. There exist two main sources of disturbances in the hard disk drive dynamics. The first is denominated *repeatable runout* (RRO), which is produced by imperfections and eccentricities on the tracks. The second is *non–repeatable runout* (NRRO), produced by the aggregated effects of disk drive vibrations, electrical noise in the circuits and the measurement channels.

Model–based noise rejection adaptive schemes are well suited to deal with the problems previously described here. There exist a series of slightly different model–based adaptive methods, being the *adaptive inverse control* (AIC) [4] and the *adaptive–Q* (A–Q) [5] the two most prominent schemes. Despite the different denominations, they are essentially the same. The implementation of an add–on adaptive controller for disk drives, based on the AIC scheme is described in [3]. There, the adaptive algorithm employs the classical RLS recursions in [6]. The experimental implementation of an A–Q scheme is demonstrated in [1]. There, the disk drive open–loop plant is stabilized using a *linear time–invariant* (LTI) LQG compensator and then an adaptive filter Q is added using the typical configuration in [5]. The adaptation is done using low order LMS and RLS algorithms and implemented in real time using a TMS320C67 floating point *digital signal processor* (DSP).

In [2] we showed that using the frequency weighting adaptive structure in [7], and adaptive methods such as the inverse QR–RLS algorithm in [8] or the lattice algorithm in [9], the control performance can be significatively improved with respect to our previous implementations on the same experimental setup described in [1]. Nonetheless, analyses in the frequency domain indicate that part of the power due to RRO components still remains. To deal with this issue, in this work, we introduce a control scheme that specifically targets the RRO components in the disturbance signal. This method integrates repetitive and adaptive components based on both the idea of *internal model* [10] and *minimum variance regulation* [11]. In order to achieve this objective, the challenge was the formulation of a meaningful optimization problem that incorporated both approaches. This article reports empirical evidence on the validity of this technique, since the controller presented here achieves both a significant attenuation of the RRO components and an improvement with respect to the performance achieved by the controller presented by us in [2]. A similar method was attempted in [12], however, the results reported here are significantly better. The experimental implementation of the control system was done using a *Mathworks*® xPC Target system.

The paper is organized as follows. Section II describes the systems involved in the experiment. Section III explains the development of the adaptive–repetitive control method. Section IV reviews some aspects of the *adaptive feedforward cancelation* (AFC) method in [13] used for comparison employing the data presented in [14]. Experimental results are presented in Section V, and finally, some conclusions are drawn in Section VI.

II. Experiment and Systems

The experimental setup is identical to the one described in [2] running with a sample–and–hold rate of 9.36 KHz. The open–loop plant, denoted by P, is connected to the systems C and U_1, as shown in Fig. 1, defining closed–loop plants G_1 and G_2 respectively. Thus, when C is on and U_1 is off the mapping from u to y is G_1, and when both C and U_1 are on the mapping from u to y is G_2. The controller C was designed employing classical techniques, and U_1 is the result of a minimum–variance RLS–based tuning process, as explained

This work was supported in part by the National Science Foundation Nanoscale Science and Engineering Center for Scalable and Integrated Nanomanufacturing (SINAM) under Grant DMI 0327077.

The authors are with the Mechanical and Aerospace Engineering Department, University of California, Los Angeles, CA, 90095–1597, USA. nestor@seas.ucla.edu, chiying@seas.ucla.edu, ttsao@seas.ucla.edu, gibson@ucla.edu.

in [2]. Identified models for the open–loop plant and the two closed–loop plants, denoted by $\hat{P}$, $\hat{G}_1$ and $\hat{G}_2$, are shown *in blue*, *in green* and *in red* in Fig. 2. Also, the controllers C and $(C-U_1)$ determine the output–sensitivity functions (the mappings from w_0 to y), whose estimates $\hat{S}_C = \left(1+\hat{P}C\right)^{-1}$ and $\hat{S}_{(C-U_1)} = \left[1+\hat{P}(C-U_1)\right]^{-1}$ are shown *in blue* and *in green* in Fig. 5. Similarly, estimates for the reference–sensitivity functions (the mappings from y_{ref} to y), $\hat{N}_C = \hat{P}C\left(1+\hat{P}C\right)^{-1}$ and $\hat{N}_{(C-N_1)} = \hat{P}(C-U_1)\left[1+\hat{P}(C-U_1)\right]^{-1}$ are shown *in blue* and *in green* in Fig. 6.

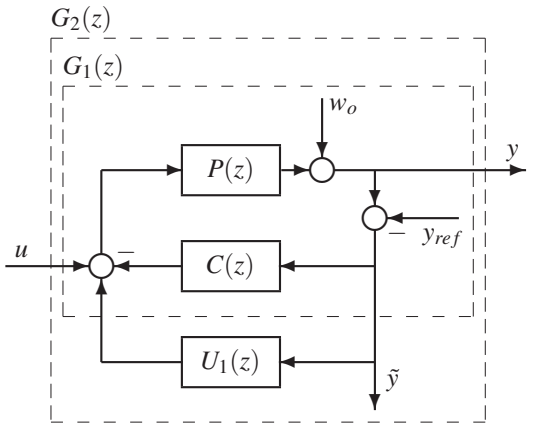

Fig. 1. Block diagram of LTI feedback control system. $P(z)$ = open–loop plant; $C(z)$ = classical LTI feedback controller; y = position of the head; u = input signal; w_o = output disturbance; y_{ref} = position reference; $\tilde{y}$ = position error; $G_1(z)$ = closed–loop plant with $C(z)$ on and $U_1(z)$ off; $G_2(z)$ = closed–loop plant with both $C(z)$ and $U_1(z)$ on.

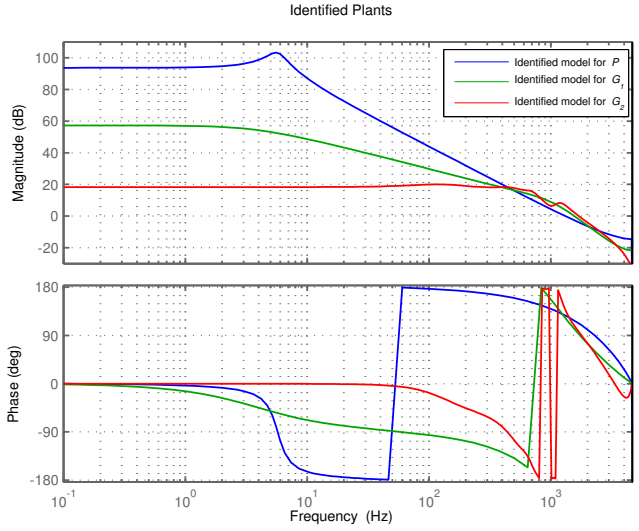

Fig. 2. Bode plot for identified plants $\hat{P}$, $\hat{G}_1$, and $\hat{G}_2$.

III. Adaptive–Repetitive Control

As it will be shown in the experimental section, the RLS–based tuned control–system U_1 is able to improve the performance TMR index significantly when compared with the performance achieved by the use of the controller C alone. However, the *power spectral densities* (PSD) indicate that the influence of the RRO disturbances is not completely counteracted by the use of $(C-U_1)$. As shown *in red* in Fig. 8, many spikes allocated at frequencies multiple of 120 Hz still remain. This suggests that an adaptive scheme that considers this information might be more effective than one that does not. Two prominent methods for dealing with RRO disturbances have been described in the literature. The first one is repetitive control, which uses the concept of *internal model* in [10] for synthesizing LTI controllers. The second method adaptively finds the Fourier coefficients corresponding to a number of given sinusoidal disturbances [13]. In this paper we introduce a control scheme that simultaneously integrates repetitive and adaptive elements.

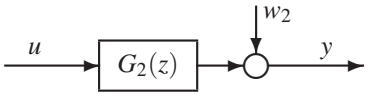

Fig. 3. Closed–loop plant G_2 and output disturbance w_2.

To begin with, we assume $\hat{G}_2 = G_2$ and we represent the aggregated effects of all the disturbances acting on the system by the output disturbance w_2, i.e., $w_2 = [1+P(C-U_1)]^{-1}w_0$. This is illustrated in Fig. 3. Then we choose the internal model $D = 1-q(z,z^{-1})z^{-N}$, where q is a zero–phase low–pass filter and N is the period of the periodical disturbance to be attenuated. Notice that the operator q allows us some flexibility over the frequency range of disturbances to be canceled while maintaining stability. The filter D has a combed shape with notches matching the frequencies of the periodic disturbance signals. Thus, ideally we would like to look for a filter K that makes the frequency respond of the LTI system $1-KG_2$ close to zero at the same periodic frequencies. This is achievable by solving the Bézout identity

$$RD+KG_2 = 1, \tag{1}$$

where R and K are the unknowns.

For the Diophantine equation in (1) the existence of solutions for R and K will be assured if G_2 and D are coprime. Furthermore, (1) characterizes a whole family of stabilizing internal model type repetitive controllers [15]. Following the general guidelines in [15] and [16] a particular solution is presented here. The method starts by separating G_2 into its minimum and non–minimum phase parts G_o and G_i respectively. Thus,

$$G_2 = \frac{B}{A} = \frac{B^+B^-}{A} = G_iG_o, \qquad G_o = \frac{B^+}{A}, \qquad G_i = B^-. \tag{2}$$

Where B^+ and B^- are the cancelable and uncancelable parts of the numerator B of G. Now, substituting (2) into (1) we can write

$$RD+K'G_i = 1, \qquad K' = KG_o. \tag{3}$$

Among the infinity many solutions to (3) it is verifiable by simple algebraic manipulations that one of the solutions is given by

$$R_o = \frac{1}{1-(1-\gamma G_i^* G_i)qz^{-N}}, \qquad (4)$$

$$K_o' = q\gamma G_i^* z^{-N} R_o, \qquad K_o = K_o' G_o^{-1}.$$

Here, G_i^* is defined as $G_i^*(z^{-1}) = G_i(z)$, and γ as a positive real number.

At this point, questions on the causality and the stability of the controller K_o arise. The zero–phase filter q is noncausal and the plants G_i and G_i^* might not be causal as well. Nonetheless, the causality of K_o is guaranteed for a sufficiently large N, since z^{-N} is a factor of both $(1-\gamma G_i^* G_i)qz^{-N}$ and $\gamma q G_i^* z^{-N}$. Also, it is verifiable, by the use of the *small gain* theorem that the stability of K_o and the stability of R_o are ensured by the sufficient condition

$$|1-\gamma G_i^*(e^{j\theta})G_i(e^{j\theta})| < \frac{1}{|q(e^{j\theta})|}, \quad \forall \quad \theta \in [0,\pi]. \qquad (5)$$

In (5) the real number γ can be thought of as a stability and performance tuning parameter. Fig. 4 shows the fulfilment of the condition (5) and the achievable performances for three different values of γ: 4.5×10^{-7}, 1.5×10^{-7} and 4.5×10^{-8}. Clearly, the deepest notches are achieved with the value 4.5×10^{-7}, at the expense of some frequency amplification on the inter–notch regions. We choose this last value because the amplified regions can be canceled adaptively as we will show later. The bottom plot in Fig. 4 shows $1-G_2K_o$, which is the sensitivity function from w_2 to y. However, what is more interesting at this point is the shape of the overall sensitivity function $S_{C-U_1-U_2} = [1+P(C-U_1-U_2)]^{-1}$ from w_o to y, and also the shape of $N_{C-U_1-U_2} = P(C-U_1-U_2)[1+P(C-U_1-U_2)]^{-1}$ from y_{ref} to y, with $U_2 = -K_o(1-K_oG_2)^{-1}$. Estimates for both transfer functions are shown *in red* in Fig. 5 and Fig. 6 respectively. Notice that this internal–model–based controller is not only able to create deep notches but also to improve the rejection over low frequencies at the expense of some amplification on inter–notch regions, that can be attenuated, anew, adaptively.

Now, consider an arbitrary asymptotically stable and rational LTI filter Q, i.e., $Q \in RH_\infty$. Also, let $R(Q) = R_o - QG_2$, and $K(Q) = K_o + QD$. Then it is clear that these R and K define an entire family of solutions to (1). Notice that R and K belong to RH_∞ for all $Q \in RH_\infty$ provided that D and G_2 are stable. This parameterization allows us to formulate the control objective as an optimization problem. Specifically we would like to minimize the variance of the random variable $\tilde{\mathbf{y}}(k)\ \forall\ k$. Thus, let $\tilde{\mathbf{y}}$ be a stationary mean– and covariance–ergodic random process for any given stable LTI filter Q. Then, the problem becomes

$$\min_{Q\in RH_\infty} E\{\tilde{\mathbf{y}}^2(k)\}. \qquad (6)$$

Notice, that if $E\{\tilde{\mathbf{y}}^2(k)\} = \sigma^2$, the ergodicity assumption implies that $\lim_{N\to\infty}\frac{1}{N}\sum_{k=0}^{N}\tilde{y}^2(k) = \sigma^2$, with probability 1.

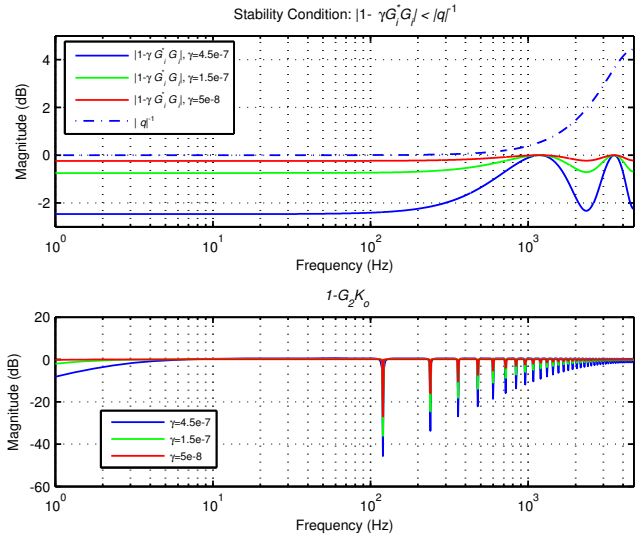

Fig. 4. *Top plot:* Sufficient stability condition for different values of γ. *Bottom plot:* Estimated sensitivity function from w_2 to y, $1-G_2K_o$, for different values of γ.

Also, it is verifiable that (6) is equivalent to the H_2 problem

$$\min_{Q\in RH_\infty} \|W_2 - G_2KW_2\|_2, \qquad (7)$$

where W_2 is a stable filter that maps a stationary, white, zero–mean, unit–variance Gaussian random sequence to the disturbance w_2. This filter is usually called *the disturbance model* of w_2. Finally, considering (1) and the parameterized systems $K(Q)$ and $R(Q)$, (7) can be re–arranged as

$$\min_{Q\in RH_\infty} \|R_oDW_2 - QG_2DW_2\|_2. \qquad (8)$$

The work we have done thus far enables us to translate the original problem into an adaptive filtering one solvable in real–time by the use of algorithms like LMS or RLS. This adaptive scheme is shown in Fig. 7. The first thing to notice is that the controller $K(Q) = K_o + QD$ can be broken into a repetitive part K_o and an adaptive part QD. The fundamental idea here is that the adaptive algorithm is ran with a regressor formed by values from the signal Dw_2 and not w_2. Thus, the RRO part of w_2 is attenuated by K_o and what is left, Dw_2, is attenuated adaptively. For this work we choose to implement the LMS and inverse QR–RLS algorithms in [8]. Thus, first we introduce the constrain $Q(z) = \sum_{i=0}^{N_o}\theta_i z^{-i}$, where N_o is the order of the filter. Then, using LMS, (6) can be approximated iteratively via the recursion

$$\theta(k) = \theta(k-1) + \mu\Psi^T(k)[\delta(k) - \Psi(k)\theta(k-1)], \qquad (9)$$

with $k \geq 0$, $\theta(-1) = 0$, $\theta(k) = [\theta_0(k)\ \cdots\ \theta_{N_o}(k)]^T$, the desired value $\delta(k) = R_oD\hat{w}_2(k)$, the regression matrix $\Psi(k) = [\hat{G}_2D\hat{w}_2(k)\ \cdots\ \hat{G}_2D\hat{w}_2(k-N_o)]$, and the positive step–size μ. Similarly, the inverse QR–RLS algorithm can be implemented by forming the same $\Psi(k)$ and $\delta(k)$.

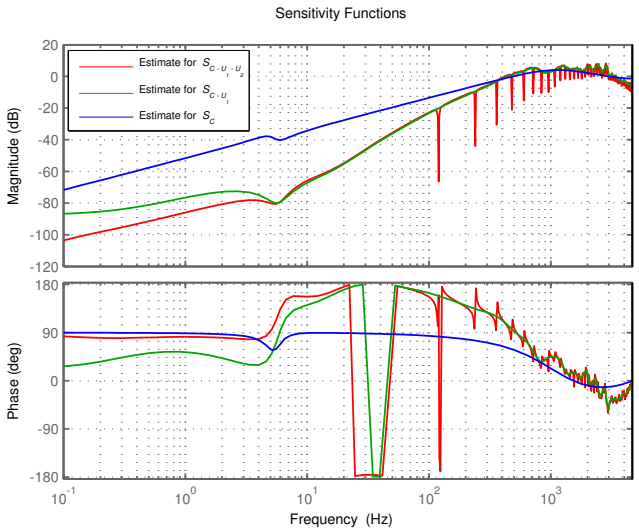

Fig. 5. Bode plots for the computed output sensitivity transfer functions $\hat{S}_C = \left(1+\hat{P}C\right)^{-1}$, $\hat{S}_{C-U_1} = \left[1+\hat{P}(C-U_1)\right]^{-1}$, and $\hat{S}_{C-U_1-U_2} = \left[1+\hat{P}(C-U_1-U_2)\right]^{-1}$.

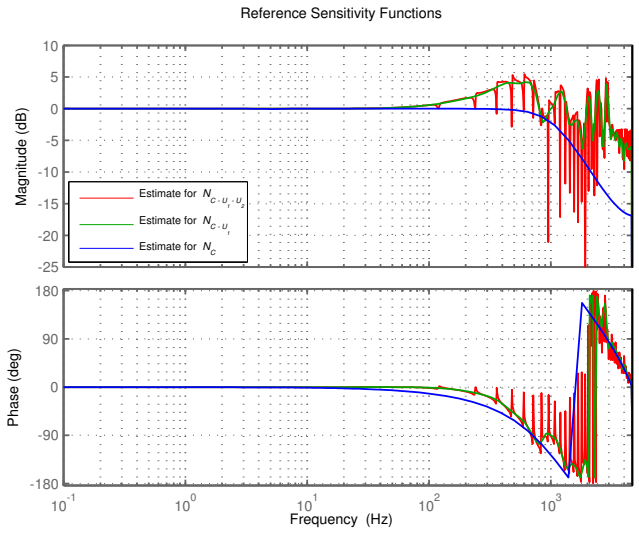

Fig. 6. Bode plots for the computed mappings $\hat{N}_1(z)$, $\hat{N}_2(z)$ and $\hat{N}_3(z)$ from y_{ref} to y, for controllers C, $C-U_1$, and $C-U_1-U_2$ respectively.

IV. Review of the Adaptive Feedforward Cancelation Method

In order to validate the method developed here, we compare the experimental results with the ones presented in [14], obtained by the use of the so–called *adaptive feedforward cancelation* (AFC) method in [13]. In this case, the RRO occurs at frequencies $120m$ Hz, with $m = 1,2,\ldots,n_{max}$ due to the 7200 rpm speed of the disk. Here, we consider the closed–loop plant G_2 and we assume that this is subjected to the output disturbance $d = w_2$ consisting of a linear combination of harmonic signals with the fundamental frequency of 120 Hz, i.e.,

$$d(k) = \sum_{i=1}^{n_{max}} \left\{ a_i(k)\sin\left(\frac{2\pi ik}{N_{rev}}\right) + b_i(k)\cos\left(\frac{2\pi ik}{N_{rev}}\right)\right\}, \quad (10)$$

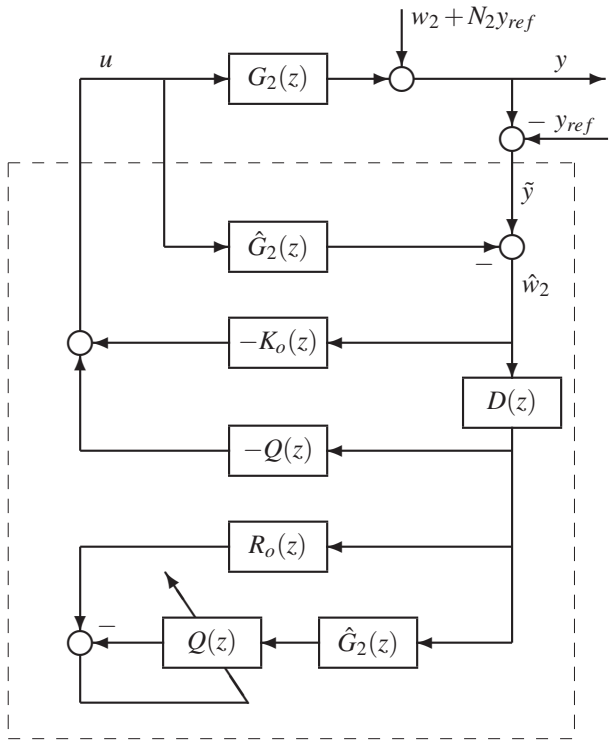

Fig. 7. Adaptive–repetitive control scheme.

where i is the index for the harmonic and N_{rev} is the number of samples per revolution. Thus, the idea is to adaptively generate a control signal u, such that, the output G_2u would cancel the disturbance d. Here, we slightly modify the algorithm in [13] to achieve that objective. To begin with, notice that if the whole system is modeled as in Fig. 3, then the output would be $y(k) = [G_2u](k) + d(k)$. Then, in order to cancel the disturbance, the control signal should satisfy that

$$[G_2u](k) = -\hat{d}(k), \quad (11)$$

where $\hat{d}(k)$ is an estimate for the RRO disturbance $d(k)$, which is adaptively updated. Recalling that d is formed by finite linear combinations of sines and cosines, the control signal u has the same structure, i.e., it consists of a finite sum of sines and cosines. Therefore, the effect of G_2 over u is that each harmonic component of u will be modified in phase and amplitude. The phase modification can be estimated off–line through system identification. The amplitude modification is irrelevant, since it can be implicitly estimated. Thus, the algorithm in [13] to generate $u(k)$, modified for our case, becomes

$$u(k) = -\hat{d}_{RRO}(k) \quad (12)$$

$$\hat{d}_{RRO}(k) = \sum_{i=1}^{n_{max}} \left\{ \hat{a}_i(k)\sin\left(\frac{2\pi ik}{N_{rev}}\right) + \hat{b}_i(k)\cos\left(\frac{2\pi ik}{N_{rev}}\right)\right\} \quad (13)$$

$$\hat{a}_i(k) = \hat{a}_i(k-1) + \gamma_i y(k-1)\sin\left(\frac{2\pi ik}{N_{rev}} + \phi_i\right) \quad (14)$$

$$\hat{b}_i(k) = \hat{b}_i(k-1) + \gamma_i y(k-1)\cos\left(\frac{2\pi ik}{N_{rev}} + \phi_i\right). \qquad (15)$$

Where the γ_i are adaptation gains, chosen differently for each harmonic. The angle $\phi_i = \angle G_2(e^{j\omega_i})$ is the phase modification added in order to compensate the effect of G_2 on u, with ω_i being the angular frequency of the i^{th} harmonic. For stability analysis and other details concerning the algorithm see [13]. The explanation presented in this section is largely based on [14].

V. Experimental Results

In the experiments presented here, the sample–and–hold rate was 9.36 KHz, externally determined by the HDD clock. The controller U_1 is computed as $U_1 = F_o(1 + F_o\hat{G}_1)^{-1}$, where F_o is a 36^{th} order filter tuned on the position *head* 0–*track* 15,000 as described in [2]. The system K_o was designed with $\gamma = 4.5 \times 10^{-7}$ and the filter K is adapted using the LMS algorithm with $N_o = 128$ and the inverse QR-RLS algorithm with orders $N_o = 16$ and $N_o = 36$. The performances, quantified by the 3σ index, obtained at different positions of the HDD are shown in Table I, which contains an extended version of the results in [17]. In all cases the results achieved by the adaptive–repetitive controller are better compared to the ones achieved by the use of the combined LTI controller $(C - U_1)$ alone, and also by the combined controller $(C - U_1 - U_2)$ alone. In order to validate the adaptive–repetitive method, we contrast the obtained results with the ones obtained by the use of the AFC method. As shown in Table I, for the case in which we use the inverse QR–RLS algorithm with order 36 the results are similar to the ones achieved using the AFC method. However, from a computational point of view, the method presented here is significantly simpler. Also, it is important to emphasize that the AFC–based controller is added to $(C - U_1)$, which explains to a great extend the high performance achieved. We refer to the controller based on the AFC method as K_{RRO}.

Fig. 8 shows time series, *power spectral densities* (PSDs), histograms and a deviation graph, for a experiment at the location *head* 0–*track* 15,000, using a 128^{th} order LMS filter. The plots show *in blue* all curves corresponding to the signal $\tilde{y}$ for the system under the LTI controller C, *in red* all curves corresponding to the signal $\tilde{y}$ for the system under the LTI controllers C and F_o, i.e., $(C - U_1)$, and *in green* all curves corresponding to the signal $\tilde{y}$ for the system under the controllers C, F_o and K (adaptive–repetitive). The curves for the system under the controllers C, F_o and K_o, i.e., $(C - U_1 - U_2)$ are omitted. The time series sharply show the difference that the controller F_o makes with respect to the controller C alone. The difference between the controller F_o and K is more subtle, nevertheless this can be fully appreciated in the comparison of the PSDs, being clear that the objective of targeting the RRO components in the disturbance has been accomplished, which is emphasized by the close–ups in Fig. 9. Also, as predicted by the comparison of the sensitivity functions in Fig. 5 the improvement in terms of the 3σ value is explained by two elements, the attenuation of the RRO components and the further reduction of the low frequency content. The two bottom plots in Fig. 8 compare the data statistically. Both, the histograms, and the deviation from the center graph, simply show that the adaptive–repetitive K controller makes the data to concentrate closer to the center of the track when compared with the former controllers.

VI. Conclusions

This paper presented a control scheme intended to target both, the NRRO and RRO components of the disturbance to which a HDD is subjected. This scheme unites the design methodology in [2] with the synthesis of a controller that integrates repetitive and adaptive components by the formulation of an appropriate optimization problem. Experimental results were presented to demonstrate the effectiveness of this approach.

References

[1] K. Krishnamoorthy and T.-C. Tsao, "Adaptive-Q with LQG Stabilization Feedback and Real Time Computation for Disk Drive Servo Control," in *Proc. of the American Control Conference*, Boston, MA, Jun. 2004, pp. 1171–1175.

[2] N. O. Pérez Arancibia, T.-C. Tsao, and S. Gibson, "Adaptive Tuning and Control of a Hard Disk Drive," in *Proc. of the American Control Conference*, New York, NY, Jun. 2007, pp. 1526–1531.

[3] R. Horowitz and B. Li, "Adaptive Control for Disk File Actuators," in *Proc. 34th IEEE Conf. on Decision and Control*, New Orleans, LA, Dec. 1995, pp. 655–660.

[4] B. Widrow and E. Walach, *Adaptive Inverse Control*. Upper Saddle River, NJ: Prentice-Hall, 1996.

[5] T.-T. Tay, I. Mareels, and J. B. Moore, *High Performance Control*. Boston, MA: Birkhäuser, 1998.

[6] G. C. Goodwin and K. S. Sin, *Adaptive Filtering, Prediction and Control*. Englewood Cliffs, NJ: Prentice-Hall, 1984.

[7] N. O. Pérez Arancibia, S. Gibson, and T.-C. Tsao, "Saturation and frequency weighting in adaptive control of laser beam jitter," in *Proc. SPIE 6709, Free–Space Laser Communications VII*, San Diego, CA, Aug. 2007, 6709–27.

[8] A. H. Sayed, *Fundamentals of Adaptive Filtering*. New York, NY: Wiley, 2003.

[9] S.-B. Jiang and J. S. Gibson, "An unwindowed multichannel lattice filter with orthogonal channels," *IEEE Transactions on Signal Processing*, vol. 43, no. 12, pp. 2831–2842, Dec. 1995.

[10] B. A. Francis and W. M. Wonham, "The internal model principle of control theory," *Automatica*, vol. 12, no. 5, pp. 457–465, Sept. 1976.

[11] R. Horowitz, B. Li, and J. W. McCormick, "Wiener-filter-based Minimum Variance Self-tuning Regulation," *Automatica*, vol. 34, no. 5, pp. 531–544, May 1998.

[12] K. Krishnamoorthy and T.-C. Tsao, "Robust Adaptive-Q with Two Period Repetitive Control for Disk Drive Track Following," in *Proc. ASME International Conference on Advanced Intelligent Mechatronics*, Monterey, CA, Jul. 2005, pp. 13–18.

[13] A. Sacks, M. Bodson, and P. Khosla, "Experimental Results of Adaptive Periodic Disturbance Cancellation in a High Performance Magnetic Disk Drive," *ASME Journal of Dynamic Systems, Measurement, and Control*, vol. 118, no. 3, pp. 416–424, Sept. 1996.

[14] J. Levin, N. O. Pérez Arancibia, P. A. Ioannou, and T.-C. Tsao, "Adaptive Disturbance Rejection for Disk Drives Using Neural Networks," submitted to *the American Control Conference*, Seattle, WA, Jun. 2008.

[15] M. Tomizuka, T.-C. Tsao, and K.-K. Chew, "Analysis and Synthesis of Discrete-Time Repetitive Controllers," *ASME Journal of Dynamic Systems, Measurement, and Control*, vol. 111, no. 3, pp. 353–358, Sept. 1989.

[16] M. Tomizuka, "Zero Phase Error Tracking Alagorithm for Digital Control," *ASME Journal of Dynamic Systems, Measurement, and Control*, vol. 111, no. 1, pp. 65–68, Mar. 1987.

[17] N. O. Pérez Arancibia, C.-Y. Lin, S. Gibson, and T.-C. Tsao, "Adaptive and Repetitive Control for Rejecting Repeatable and Non–repeatable Runout in Rotating Devices," in *Proc. ASME International Mechanical Engineering Congress and Exposition*, Seattle, WA, Nov. 2007, IMECE2007–43534.

TABLE I

3σ VALUE OF THE POSITION ERROR SIGNAL (PES) AS A PERCENTAGE OF THE TRACK WIDTH

	Head 0			Head 1			Head 2		
	$y_{ref} = 1e4$	$y_{ref} = 1.5e4$	$y_{ref} = 2e4$	$y_{ref} = 1e4$	$y_{ref} = 1.5e4$	$y_{ref} = 2e4$	$y_{ref} = 1e4$	$y_{ref} = 1.5e4$	$y_{ref} = 2e4$
C	18.1429	17.2467	20.6328	16.3020	18.6647	22.6426	22.0292	23.3535	24.4753
$(C-U_1)$	5.3699	5.1232	5.0475	5.1924	5.4398	4.8723	5.8560	5.0029	5.6392
$(C-U_1-U_2)$	4.7114	4.5694	4.4946	4.4731	4.3640	4.1393	5.2075	4.7034	4.7845
$(C-U_1)$ & K (LMS–128)	4.6057	4.3678	4.2991	4.3663	4.2926	4.0389	5.0778	4.6138	4.7316
$(C-U_1)$ & K (I–QR–RLS–16)	4.5473	4.2583	4.2287	4.3654	4.3277	4.0187	5.0292	4.6059	4.5529
$(C-U_1)$ & K (I–QR–RLS–36)	4.4950	4.0231	4.2606	4.2891	4.1485	4.0189	4.8111	4.4386	4.3762
$(C-U_1)$ & K_{RRO} (AFC)	4.3427	4.0704	4.1812	4.4606	4.2179	3.9496	5.0310	4.5811	4.2149

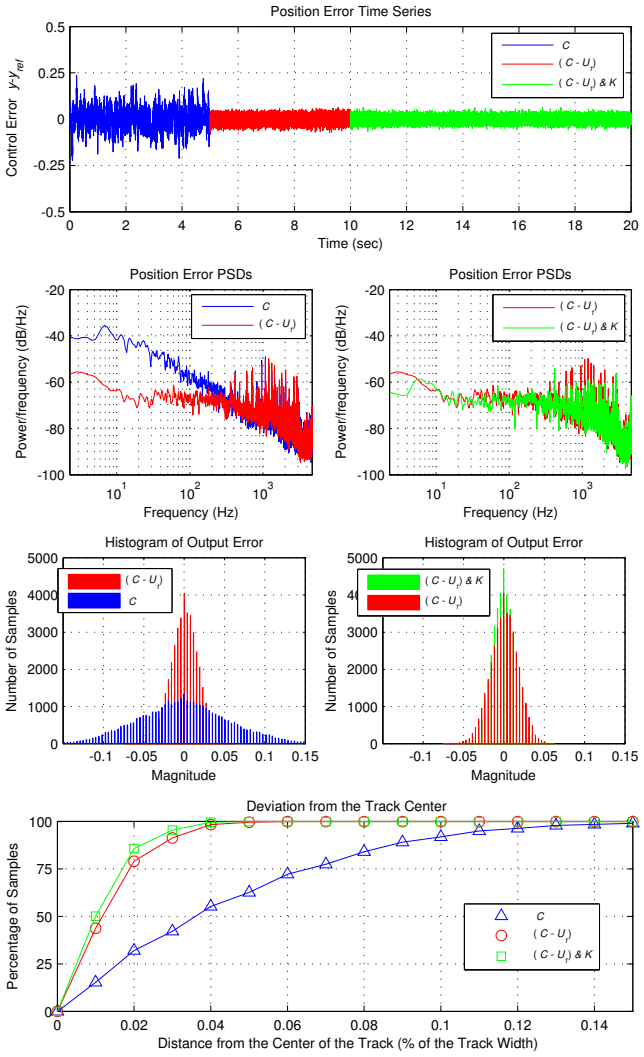

Fig. 8. Experiment performed on head 0 and track 15,000. Curves in *blue* correspond to the HDD under controller C. Curves in *red* correspond to the HDD under controllers C and F_o, i.e., $C-U_1$. Curves in *green* correspond to the HDD under controllers C, F_o, and the adaptive-repetitive controller K using a 128^{th} order LMS filter. *Top Plot:* Time series. *Second-row Plot:* PSDs. *Third-row plot:* Histograms. *Bottom Plot:* Deviation from the center graphs. This plot shows, in percentage, the number of samples inside a certain distance from the center of the track.

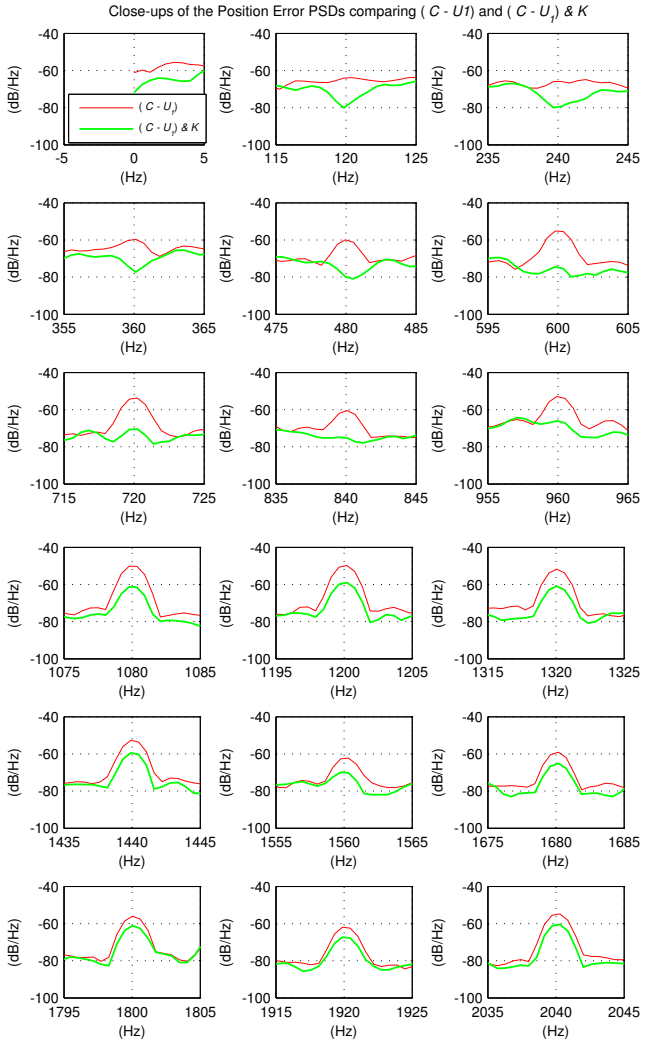

Fig. 9. Experiment performed on head 0 and track 15,000. The plots show close-ups of the PSDs comparing the performance of the HDD system under controllers C and F_o, i.e., $C-U_1$ and under C, F_o and the adaptive-repetitive controller K. Since the spikes due to RRO are at frequencies $120m$ Hz, $m = 0,\ 1,\ 2,\ \cdots$, and the Nyquist frequency is 4680, the period N in $D = 1-q(z,z^{-1})z^{-N}$ is chosen to be 78. As predicted by the sensitivity functions in Fig. 5, the most significant attenuations, corresponding to the deepest notches in Fig. 5, are between 0 and 960 Hz.